

Fingerprints of heavy element nucleosynthesis in the late-time lightcurves of kilonovae

Meng-Ru Wu,^{1,2,*} J. Barnes,^{3,†} G. Martínez-Pinedo,^{4,5,‡} and B. D. Metzger^{3,§}

¹*Institute of Physics, Academia Sinica, Taipei, 11529, Taiwan*

²*Institute of Astronomy and Astrophysics, Academia Sinica, Taipei, 10617, Taiwan*

³*Department of Physics and Columbia Astrophysics Laboratory,*

Columbia University, Pupin Hall, New York, NY 10027, USA

⁴*GSI Helmholtzzentrum für Schwerionenforschung, Planckstraße 1, 64291 Darmstadt, Germany*

⁵*Institut für Kernphysik (Theoriezentrum), Technische Universität Darmstadt,*

Schlossgartenstraße 2, 64289 Darmstadt, Germany

(Dated: January 8, 2019)

The kilonova emission observed following the binary neutron star merger event GW170817 provided the first direct evidence for the synthesis of heavy nuclei through the rapid neutron capture process (r -process). The late-time transition in the spectral energy distribution to near-infrared wavelengths was interpreted as indicating the production of lanthanide nuclei, with atomic mass number $A \gtrsim 140$. However, compelling evidence for the presence of even heavier third-peak ($A \approx 195$) r -process elements (e.g., gold, platinum) or translead nuclei remains elusive. At early times (\sim days) most of the r -process heating arises from a large statistical ensemble of β -decays, which thermalize efficiently while the ejecta is still dense, generating a heating rate that is reasonably approximated by a single power-law. However, at later times of weeks to months, the decay energy input can also possibly be dominated by a discrete number of α -decays, ^{223}Ra (half-life $t_{1/2} = 11.43$ d), ^{225}Ac ($t_{1/2} = 10.0$ d, following the β -decay of ^{225}Ra with $t_{1/2} = 14.9$ d), and the fissioning isotope ^{254}Cf ($t_{1/2} = 60.5$ d), which liberate more energy per decay and thermalize with greater efficiency than beta-decay products. Late-time nebular observations of kilonovae which constrain the radioactive power provide the potential to identify signatures of these individual isotopes, thus confirming the production of heavy nuclei. In order to constrain the bolometric light to the required accuracy, multi-epoch and wide-band observations are required with sensitive instruments like the James Webb Space Telescope. In addition, by comparing the nuclear heating rate obtained with an abundance distribution that follows the Solar r abundance pattern, to the bolometric lightcurve of AT 2017gfo, we find that the yet-uncertain r abundance of ^{72}Ge plays a decisive role in powering the lightcurve, if one assumes that GW170817 has produced a full range of the Solar r abundances down to mass number $A \sim 70$.

Introduction— The gravitational wave emission detected from the binary neutron star merger (NSM) GW170817 by Advanced LIGO [1] triggered a worldwide search for electromagnetic counterparts [2]. Within eleven hours of the coalescence, a fading blue thermal source, AT 2017gfo, was discovered from the galaxy NGC 4993 [3, 4]. The luminosity and evolution agreed with predictions for the light powered by the radioactive decay of heavy nuclei synthesized via the rapid neutron capture process (r -process) in neutron-rich merger ejecta [5–8]. The presence of luminous visual wavelength (“blue”) emission at early times was interpreted by most groups as arising from the fastest outer layers of the ejecta, which contained exclusively light r -process nuclei with a relatively low visual wavelength opacity [9–11] (see, however, Ref. [12, 13]). The observed transition of the emission colors to the near-infrared confirmed predictions for the inner ejecta layers containing lanthanide elements, with atomic mass number $A \gtrsim 140$ [8, 14, 15]. The amount of the merger ejecta was estimated to be $M_{\text{ej}} \approx 0.03 - 0.06 M_{\odot}$ [12, 13, 16–19], with the bulk of which expanding at velocities of $v_{\text{ej}} \approx 0.1$ c.

Although evidence exists for the presence of some lanthanides in the ejecta of GW170817, the detailed abundance pattern of the nuclei synthesized, and how it com-

pares to those in the Solar System or metal-poor stars, remains less clear. This uncertainty arises partly because of incomplete atomic data for the relevant elements and ionization states, as well as the modeling of radiative transfer. Even with accurate modeling, most kilonova properties at early times ~ 1 –10 days, when the lightcurves are at their peaks, are insensitive to the presence of even heavier nuclei, such as the third-peak ($A \approx 195$) r -process elements (e.g., gold, platinum) and transuranic nuclei. Lanthanides are only produced in ejecta with low electron fraction, $Y_e \lesssim 0.25$ [9, 20], while even smaller Y_e are needed to synthesize heavier isotopes. Whether the ejecta of GW170817 contained such low Y_e matter is presently unknown.

At times after ~ 10 days, the ejecta becomes transparent, entering a “nebular” phase in analogy with those of supernovae, which are observed starting months after explosion. Although the uncertainties associated with the ejecta opacity become smaller as it dilutes, these are replaced by even larger uncertainties in calculating the nebular spectrum, due to the increasing importance of deviations from local thermodynamical equilibrium (see Ref. [21] for a review in the supernova context). Nevertheless, if one could measure the *bolometric* nebular emission, it should faithfully track the radioactive decay

energy input.

Table I in the Supplemental Material (SM) lists *all* 25 r -process isotopes with half-lives of 10–100 days that can contribute to late-time heating. Given the small number of isotopes, one might hope to detect the decay signatures of individual isotopes and their associated yields, in the way that the ^{56}Ni to ^{56}Co chain is observed in normal supernovae. As we shall show, these signatures could provide useful diagnoses of the range of heavy nuclei that are produced or even the elusive definitive proof that the heaviest nuclei in the universe are synthesized in NSM.

Late-Time Kilonova Heating— We first examine the late-time kilonova emission for a few ejecta models that contain distinct nuclear compositions, as listed in Table I. In each model, the total r -process heating rate \dot{Q} in the ejecta of total mass M_{ej} and average expansion velocity v_{ej} can be formulated as

$$\dot{Q}(t) = \sum_i f_i(t) \dot{q}_i(t) M_{\text{ej}}. \quad (1)$$

It roughly equals the bolometric luminosity, L_{bol} , of the kilonova following its peak light, particularly at late-time after the ejecta becomes optically-thin. In Eq. (1), $\dot{q}_i(t)$ is the radioactive decay energy release rate per unit mass from a decay channel i , including β^- -decay, β^+ -decay/electron capture, α -decay and spontaneous fission. The thermalization efficiency $f_i(t)$ is defined by the ratio of the rate of the ejecta specific thermal energy increase to $\dot{q}_i(t)$ due to the thermalization of decay products. We assume that the material contains a Gaussian Y_e distribution, characterized by a central value $Y_{e,c}$ and a width ΔY_e . The corresponding $\dot{q}_i(t)$ is calculated using an r -process nuclear reaction network [22]. We adopt $f_i(t)$ of β^- -decay products based on detailed particle thermalization simulations [23] while model those of dominating individual nuclei based on the work of Ref. [24]. These represent an important improvement when compared with recent works [25, 26]. Detailed descriptions for the calculation of $\dot{q}_i(t)$ and $f_i(t)$ are given in the SM.

TABLE I. Late-time kilonova models (see text for explanations).

Model	$Y_{e,c}$	ΔY_e	A_{peak}	$M_{\text{ej}}(M_{\odot})$	$v_{\text{ej}}(c)$	Nuc. Mass.
A	0.15	0.04	130 & 195	0.040	0.1	FRDM
B	0.25	0.04	80 & 130	0.040	0.1	FRDM
C	0.35	0.04	80	0.055	0.1	FRDM
D	0.45	0.04	60	0.030	0.1	FRDM
A1	0.15	0.04	130 & 195	0.020	0.1	DZ31

For models A–D, we vary the ejecta Y_e distribution such that the produced peak and range of nuclei are largely distinct (see Table I and Fig. 1). Both model A and B with lower $Y_{e,c} = 0.15$ and 0.25 produce a wide range of nuclei across the two corresponding abundance

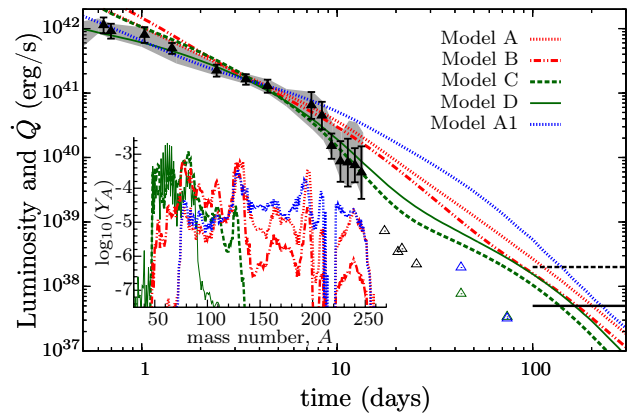


FIG. 1. L_{bol} of the kilonova associated with GW170817 from Ref. [27] (filled black triangles), including uncertainties (grey band) derived from the range of values given in Ref. [12, 18, 27]. Also shown are lower limits (empty triangles) on the late-time luminosity as inferred from the Ks band with VLT/HAWK-I [28] (black) and the $4.5 \mu\text{m}$ detections by the *Spitzer Space Telescope* from Ref. [29] (green) and Ref. [30] (blue). Colored lines show the ejecta heating rate $\dot{Q}(t)$ for different models listed in Table I. Their corresponding abundance distributions at $t = 1$ d are shown in the inset. The black solid (dashed) horizontal lines in the lower right corner represent the approximate observation limits of the NIR (MIR) instruments on the JWST for a merger at 100 Mpc.

peaks, A_{peak} . On the other hand, model C and D with higher $Y_{e,c} = 0.35$ and 0.45 only produce a smaller range of nuclei around its $A_{\text{peak}} = 80$ and 60 .

Fig. 1 shows the inferred L_{bol} of AT 2017gfo and the heating rate $\dot{Q}(t)$ derived with models A–D. We vary the M_{ej} to match the normalization of the luminosity at ~ 3 –6 days. Note that as we focus on the bulk of the ejecta, we ignore the early time data which most likely originated from a fast-moving component with different composition and lower mass. Fig. 1 shows clearly that the L_{bol} evolution in models that produce broad ranges of nuclei (A & B) starts to diverge from those with narrow ranges (C & D) at ~ 7 days. In particular, the latter cases show a clear dip at ~ 25 days. This difference originates from the number of nuclei that can decay on timescales greater than \sim days in each model. Both model A & B contain ~ 10 nuclear species that can decay at late times between 10–100 days, such that at any given time t one can find a nucleus with a commensurate β -decay lifetime $t_{1/2} \sim t$ contributing to the heating. This leads to a late-time power-law behavior of $\dot{Q}(t)$ [6, 31].

However, for models C & D which only produce nuclei around their A_{peak} , the absence of nuclei with β -decay lifetimes in the range 10–50 days for $70 \leq A \leq 100$ (see Table I in the SM) results in the observed light curve dips at ~ 25 days. Note that in both cases, the resulting $\dot{Q}(t)$ are compatible with the $L_{\text{bol}}(t)$ of

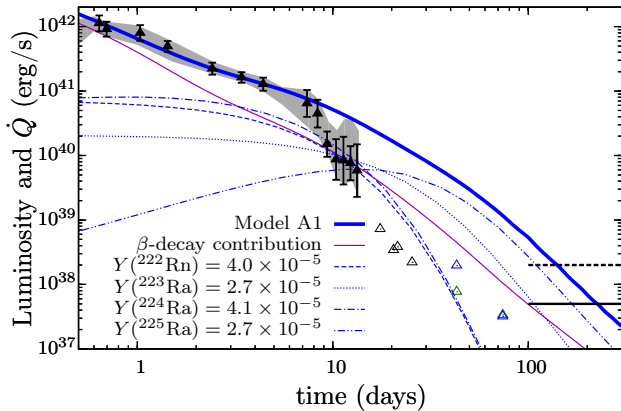


FIG. 2. Lightcurve for the model A1 (thick solid blue line) showing the dominating contributions to the total radioactive heating: beta decays (thin maroon line) and individual α -decays (thin blue lines).

AT 2017gfo and cannot be ruled out by such comparison alone (c.f., Ref. [32] which assumed single- Y_e models). A well-measured $L_{\text{bol}}(t)$ for future events covering 10–50 days can be used to infer the range of nuclei being produced in NSM. Therefore, it can provide complementary information about the nuclear composition, in addition to the inferred mass fraction of lanthanides and actinides derived from comparison to radiation transport models, due to their high opacities that results in the reddening of the spectra [8, 15].

Models A–D use the same set of nuclear reactions. Previous studies show that the choice of theoretical nuclear physics inputs can affect significantly the kilonova lightcurves [23, 33] for low Y_e ejecta, as the r -process involves extremely neutron-rich nuclei, whose key properties (masses, β -decay half-lives, ...) are not yet experimentally measured. Particularly important are the produced amount of translead nuclei that can undergo α -decays or spontaneous fission at \gtrsim days. As they release a relatively large amount of energy per decay and their decay products thermalize more efficiently than those of β -decays, they can dominate the heating even in trace amounts. Here, we illustrate the nuclear physics impact using two sets of neutron-capture rates [34] which employ, respectively, nuclear masses from the Finite-Range-Droplet-Model (FRDM) [35] for models A–D and the Duflo-Zuker parameterization with 31 parameters (DZ31) [36] for model A1.

Model A1 produces translead nuclei with $220 \lesssim A \lesssim 230$ at the level of a few times 10^{-5} , a factor of ~ 4 – 10 more than those by model A (see Fig. 1). Among those, four nuclei have α -decay half-lives between 1 and 100 days: ^{222}Rn ($t_{1/2} = 3.8$ days), ^{223}Ra ($t_{1/2} = 11.4$ days), ^{224}Ra ($t_{1/2} = 3.6$ days), and ^{225}Ac ($t_{1/2} = 10$ days), following the β -decay of ^{225}Ra with $t_{1/2} = 14.9$ days). Their

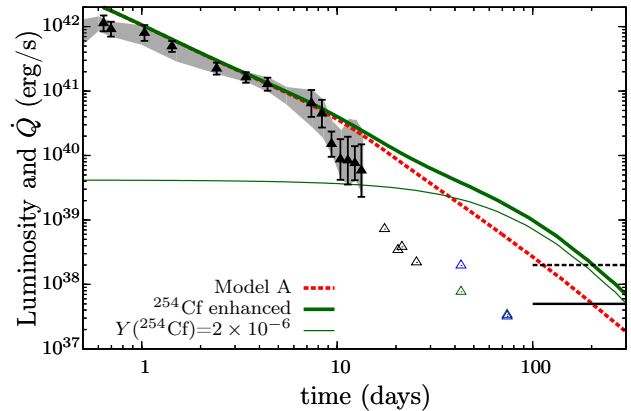


FIG. 3. The decay of ^{254}Cf could produce a late-time plateau in the lightcurve. This figure is the same as Fig. 1, but showing both the model A and a case with the ^{254}Cf abundance artificially enhanced.

decay chains release a large amount of nuclear energy ~ 30 MeV (see Table I in SM), most of which goes into the kinetic energy of α particles, that thermalize more efficiently than β -decay products. These α -decays can therefore compete with the β -decays of many other nuclei at early time ($t \sim 2$ – 6 days) and dominate the heating rate at late times, despite the abundances. We find that the enhanced heating from α -decays reduces the required M_{ej} to account for the AT 2017gfo luminosity around 3–6 days by roughly a factor of 2 (see Table I). More importantly, it generates a broad “bump”-like feature at $t \approx 6$ – 200 days that is otherwise absent without actinide production. This feature is mostly driven by the $A = 225$ decay chain due to its effective long $t_{1/2}$ (see Fig. 2). As no other radioactive nuclei can release similar energy on this timescale, such a feature in future kilonova observations would uniquely point to the production of heavy nuclei up to the actinides in that mass range to the abundance level of a few times 10^{-5} . We also note that the steepening of the AT 2017gfo L_{bol} at $t \sim 10$ d, places an upper limit of $\lesssim 10^{-5}$ for the total abundance of translead nuclei with $A = 222$ – 225 . This constraint may also be used to derive upper limits on the U and Th production in GW170817 and future NSM (see SM).

Beyond the energy deposition from α -decays, the potential importance of spontaneous fission heating was pointed out in Ref. [37] (also see Ref. [25] for a very recent work discussing the impact of ^{254}Cf fission on the lightcurve). Similar to the α -decay nuclei, whether ^{254}Cf (or even heavier nuclei) can dominantly contribute to kilonova heating is subject to nuclear physics uncertainties. The production of α -decay nuclei is sensitive to the evolution of the $N = 162$ subshell closure for $Z \sim 80$ while the amount of ^{254}Cf (and neighboring nuclei) remaining at days is sensitive to the prediction of fission barriers that affect various fission rates of the

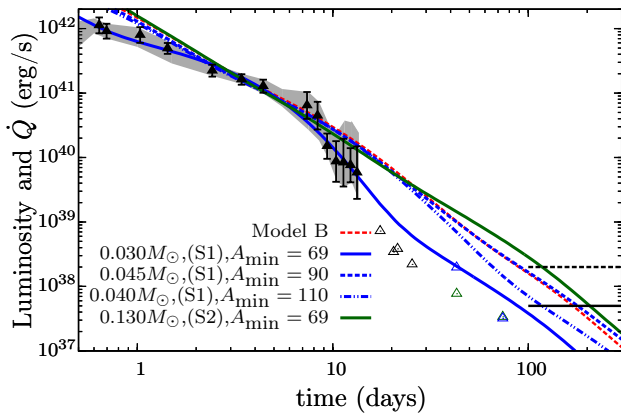


FIG. 4. The radioactive decay heating rate powered by the Solar- r abundance distribution for nuclei between A_{\min} and 205. We use two different abundance sets from [42, 43]. See text for discussions.

progenitor nuclei [38]. Within our adopted nuclear input, we do not find a significant contribution of ^{254}Cf to the heating rate when averaged over a wide range of Y_e (see Fig. 1 for the low abundance of $A \gtrsim 250$). Instead, we explore such an effect by artificially including a fraction $Y(^{254}\text{Cf}) = 2 \times 10^{-6}$ on top of the model A. Fig. 3 shows that even such a tiny quantity of ^{254}Cf ($t_{1/2} = 60.5$ days) produces a lightcurve “bump” between 50–300 days. We find that this feature can be distinguished from that due to the late-time radioactive decay of ^{56}Co ($t_{1/2} = 77.24$ days), due to the very inefficient thermalization of the ^{56}Co decay products dominated by γ -rays [39]. Note that a future identification of a “bump” feature that does not match the timescale by α -decay or ^{254}Cf fission discussed above may suggest the production of yet-unknown long-lived superheavy nuclei.

Heating from Solar r -abundances— One can ask whether the GW170817 kilonova is consistent with that expected for ejecta containing r -process nuclei with the Solar abundance pattern. From detailed multi-band lightcurve and spectral analyses, the inferred Lanthanide mass fraction, X_{lan} , is $\sim 10^{-3}$ – 10^{-2} [12, 16, 40]. Assuming that the GW170817 yield follows the Solar proportions, such low X_{lan} requires the production of all r -process nuclei with additional contributions of trans-iron nuclei

We approach this question from the viewpoint of comparing the luminosity of AT 2017gfo to the radioactive heating rate $\dot{Q}(t)$, calculated under the assumption that the only heating contribution is from β -decays and that the relative abundances of the unstable nuclei follow exactly the Solar r -abundances ratios between some minimum mass number A_{\min} and $A_{\max} = 205$ [41]. We employ two sets of the Solar r -abundances from Ref. [42] (S1) and Ref. [43] (S2).

Fig. 4 shows that with $A_{\min} = 90$ or 110, the result-

ing \dot{Q} roughly matches L_{bol} of AT 2017gfo for $M_{\text{ej}} \simeq 0.04 M_{\odot}$. In fact, they closely resemble the model B prediction and both S1 and S2 give consistent results. However, such abundance patterns would have $X_{\text{lan}} \gtrsim 0.1$, which is inconsistent with spectral modeling of AT 2017gfo.

If we instead consider that GW170817 produced the Solar r -process pattern down to $A_{\min} = 69$ (in order to reduce X_{lan} to values consistent with spectral modeling), for the S1 abundances the resulting \dot{Q} can also be consistent with the L_{bol} of AT 2017gfo. This model, however, diverges from the $A_{\min} = 90$ or 110 light curves beyond 10 d, a difference testable in future events. On the other hand, adopting the S2 abundances requires an uncomfortably large $M_{\text{ej}} \gtrsim 0.13 M_{\odot}$ to match the observed L_{bol} . This large difference arises because the abundance of ^{72}Ge in S1 is similar to its neighboring nuclei, ^{70}Zn and ^{74}Ge , while for S2 the ^{72}Ge abundance is zero. The only nucleus between $A = 69 - 90$ that contributes significantly to the heating is the decay sequence, ^{72}Zn ($t_{1/2} = 1.94$ days) to ^{72}Ga ($t_{1/2} = 0.59$ days) to ^{72}Ge , that releases a net energy ~ 3.5 MeV per decay. The β -decay contribution of ^{72}Zn in S1 thus gives rise to the bump feature at 2–5 days that is lacking for the S2 set. By artificially varying the $A = 72$ mass fraction, we find that at least $\gtrsim 20\%$ of its S1 abundance is needed match the GW170817 light curve for $M_{\text{ej}} \lesssim 0.05 M_{\odot}$ (see SM for details).

Taken together, we conclude that GW170817 may have produced a solar-like r -process yield down to $A \sim 70$, if the solar r -process contribution to the ^{72}Ge abundance is larger than $\sim 20\%$ of the value given by S1. However, if the Solar r abundance of ^{72}Ge abundance turns out to be much smaller than that of ^{70}Zn and ^{74}Ge , then either a substantial additional heating from $A < 69$ isotopes (e.g., ^{66}Ni , see [26]) would be required to make GW170817 consistent with the Solar abundances, or one would require enhanced lighter nuclei yields in $A \sim 90 - 130$ relative to the heavier nuclei beyond the second peak, when compared to the Solar r -abundances, to give $X_{\text{lan}} \lesssim 0.01$. We note, however, that the correlation of the abundances of Ge and Fe in metal-poor stars and the non-correlation of Ge and Eu [44] hints that NSM are unlikely to produce the entire solar r abundances down to $A \approx 70$.

Discussion— Our results demonstrate how late-time bolometric kilonova lightcurves can provide an important diagnostic of the nuclear composition of the NSM ejecta. Recently, Ref. [29, 30] reported detections of GW170817 at 43 and 74 days post-merger in the wavelength band centered at $4.5 \mu\text{m}$ using the *Spitzer Space Telescope*; the $3.6 \mu\text{m}$ band was also observed, resulting in non-detections. Interpreted as blackbody emission, the observed colors indicate that the ejecta had cooled by these late times to temperatures $\lesssim 1200$ K. Unfortunately, the ejecta during the nebular phase radiate through discrete spectral lines rather than as a blackbody, and so trans-

lating these observations into a bolometric luminosity is challenging. Making the very conservative assumption of counting only the luminosity in the detected band, these lower limits (shown as open triangles in Fig. 1–4) are not constraining in most of the cases. The only exception is the scenario with heating powered by solar r -abundances with $A_{\min} = 69$ with the abundance set S1, for which the late-time lightcurve is in tension with the data at 43 days of Ref. [30].

Observations of future merger events by, e.g., the James Webb Space Telescope (JWST) could be more promising [29]. For a merger at 100 Mpc, the NIRcam instrument on JWST could detect luminosities in the $\approx 0.6\text{--}4\ \mu\text{m}$ band down to $L_{\text{NIR}} \approx 5 \times 10^{37}\ \text{erg s}^{-1}$ (for a $S/N = 10$ detection given a $10^4\ \text{s}$ integration), sufficient to distinguish various models shown in, e.g., Fig. 1 out to timescales of months. The Mid-Infrared Instrument (MIRI) sensitive in the $5\text{--}14\ \mu\text{m}$ band, could constrain the luminosity to $L_{\text{MIR}} \approx 2 \times 10^{38}\ \text{erg s}^{-1}$. We emphasize that *well time-sampled* observations, which cover as wide an optical/infrared frequency range as possible, will be necessary to constrain the bolometric lightcurve evolution with sufficient precision to distinguish the nuclear physics features discussed here.

A number of uncertainties could affect future nebular measurements, which requires additional theoretical modeling. The ejecta may not radiate the radioactive heating it receives with complete efficiency. Empirically, the lightcurves of Type Ia supernovae faithfully track the radioactive decay input up to several years [45]. However, at later times the situation is less clear; non-thermally excited ions might absorb a large fraction of the radioactive energy, but due to the low density the rate of recombination could be slow and the energy released much later than injection (“freeze-out”; [46]). Freeze-out sets in on timescales of years in supernovae (see Fig. 7 of Ref. [45]), which, if occurring at the same density in a NSM, would translate into an even earlier timescale of weeks to months due to their lower ejecta mass and faster expansion speeds.

The authors acknowledge useful discussions with Andrei Andreyev, Ben Gibson, Karlheinz Langanke, Karl-Heinz Schmidt and Friedrich-Karl Thielemann, as well as anonymous referees for their helpful comments. M.-R.W. acknowledges support from the Ministry of Science and Technology, Taiwan under Grant No. 107-2119-M-001-038. J.B. is supported by the National Aeronautics and Space Administration (NASA) through the Einstein Fellowship Program, grant number PF7-180162. G.M.-P. is partly supported by the Deutsche Forschungsgemeinschaft (DFG, German Research Foundation) - Projektnummer 279384907 - SFB 1245. B.D.M. acknowledges support from NASA through the Astrophysics Research Program, grant number NNX16AB30G. Computations were partly performed on the LOEWE-CSC computer managed by Center for Scientific Computing of

the Goethe University Frankfurt. We thank the ExtreMe Matter Institute EMMI at GSI, Darmstadt, for support in the framework of the EMMI Rapid Reaction Task Force “The physics of neutron star mergers at GSI/FAIR” during which this work has been initiated.

* mwu@gate.sinica.edu.tw

† jlb2331@columbia.edu; NASA Einstein Fellow

‡ g.martinez@gsi.de

§ bdm2129@columbia.edu

- [1] B. P. Abbott *et al.* (LIGO Scientific Collaboration and Virgo Collaboration), *Phys. Rev. Lett.* **119**, 161101 (2017).
- [2] B. P. Abbott *et al.*, *Astrophys. J.* **848**, L12 (2017).
- [3] D. A. Coulter *et al.*, *Science* **358**, 1556 (2017).
- [4] M. Soares-Santos *et al.* (Dark Energy Camera GW-EM Collaboration), *Astrophys. J.* **848**, L16 (2017).
- [5] L. Li and B. Paczyński, *Astrophys. J.* **507**, L59 (1998).
- [6] B. D. Metzger, G. Martínez-Pinedo, S. Darbha, E. Quataert, A. Arcones, D. Kasen, R. Thomas, P. Nugent, I. V. Panov, and N. T. Zinner, *Mon. Not. Roy. Astr. Soc.* **406**, 2650 (2010).
- [7] L. F. Roberts, D. Kasen, W. H. Lee, and E. Ramirez-Ruiz, *Astrophys. J. Lett.* **736**, L21 (2011).
- [8] J. Barnes and D. Kasen, *Astrophys. J.* **775**, 18 (2013).
- [9] B. D. Metzger and R. Fernández, *Mon. Not. Roy. Astron. Soc.* **441**, 3444 (2014).
- [10] M. Nicholl *et al.*, *Astrophys. J.* **848**, L18 (2017).
- [11] M. R. Drout *et al.*, *Science* **358**, 1570 (2017).
- [12] E. Waxman, E. Ofek, D. Kushnir, and A. Gal-Yam, ArXiv e-prints (2017), [arXiv:1711.09638](https://arxiv.org/abs/1711.09638) [astro-ph.HE].
- [13] K. Kawaguchi, M. Shibata, and M. Tanaka, *Astrophys. J.* **865**, L21 (2018), [arXiv:1806.04088](https://arxiv.org/abs/1806.04088) [astro-ph.HE].
- [14] D. Kasen, N. R. Badnell, and J. Barnes, *Astrophys. J.* **774**, 25 (2013).
- [15] M. Tanaka and K. Hotokezaka, *Astrophys. J.* **775**, 113 (2013).
- [16] D. Kasen, B. Metzger, J. Barnes, E. Quataert, and E. Ramirez-Ruiz, *Nature* **551**, 80 (2017).
- [17] M. M. Kasliwal, E. Nakar, L. P. Singer, D. L. Kaplan, D. O. Cook, A. Van Sistine, R. M. Lau, C. Fremling, O. Gottlieb, J. E. Jencson, S. M. Adams, U. Feindt, K. Hotokezaka, S. Ghosh, D. A. Perley, P.-C. Yu, T. Piran, J. R. Allison, G. C. Anupama, A. Balasubramanian, K. W. Bannister, J. Bally, J. Barnes, S. Barway, E. Bellm, V. Bhalerao, D. Bhattacharya, N. Blagorodnova, J. S. Bloom, P. R. Brady, C. Cannella, D. Chatterjee, S. B. Cenko, B. E. Cobb, C. Copperwheat, A. Corsi, K. De, D. Dobie, S. W. K. Emery, P. A. Evans, O. D. Fox, D. A. Frail, C. Frohmaier, A. Goobar, G. Hallinan, F. Harrison, G. Helou, T. Hinderer, A. Y. Q. Ho, A. Horesh, W.-H. Ip, R. Itoh, D. Kasen, H. Kim, N. P. M. Kuin, T. Kupfer, C. Lynch, K. Madsen, P. A. Mazzali, A. A. Miller, K. Mooley, T. Murphy, C.-C. Ngeow, D. Nichols, S. Nissanke, P. Nugent, E. O. Ofek, H. Qi, R. M. Quimby, S. Rosswog, F. Rusu, E. M. Sadler, P. Schmidt, J. Sollerman, I. Steele, A. R. Williamson, Y. Xu, L. Yan, Y. Yatsu, C. Zhang, and W. Zhao, *Science* **358**, 1559 (2017), [arXiv:1710.05436](https://arxiv.org/abs/1710.05436) [astro-ph.HE].
- [18] P. S. Cowperthwaite *et al.*, *Astrophys. J.* **848**, L17

- (2017).
- [19] V. A. Villar, J. Guillochon, E. Berger, B. D. Metzger, P. S. Cowperthwaite, M. Nicholl, K. D. Alexander, P. K. Blanchard, R. Chornock, T. Eftekhari, W. Fong, R. Margutti, and P. K. G. Williams, *Astrophys. J.* **851**, L21 (2017), arXiv:1710.11576 [astro-ph.HE].
- [20] J. Lippuner and L. F. Roberts, *Astrophys. J.* **815**, 82 (2015).
- [21] A. Jerkstrand, “Spectra of Supernovae in the Nebular Phase,” in *Handbook of Supernovae*, edited by A. W. Alsabti and P. Murdin (Springer International Publishing, Cham, 2017) pp. 795–842.
- [22] M.-R. Wu, R. Fernández, G. Martínez-Pinedo, and B. D. Metzger, *Mon. Not. Roy. Astron. Soc.* **463**, 2323 (2016).
- [23] J. Barnes, D. Kasen, M.-R. Wu, and G. Martínez-Pinedo, *Astrophys. J.* **829**, 110 (2016).
- [24] D. Kasen and J. Barnes, (2018), arXiv:1807.03319 [astro-ph.HE].
- [25] Y. Zhu *et al.*, ArXiv e-prints (2018), arXiv:1806.09724 [astro-ph.HE].
- [26] S. Wanajo, (2018), arXiv:1808.03763 [astro-ph.HE].
- [27] S. J. Smartt *et al.*, *Nature* **551**, 75 (2017).
- [28] N. R. Tanvir *et al.*, *Astrophys. J.* **848**, L27 (2017), arXiv:1710.05455 [astro-ph.HE].
- [29] V. A. Villar *et al.*, *Astrophys. J.* **862**, L11 (2018).
- [30] M. M. Kasliwal *et al.*, (2018), arXiv:1812.08708 [astro-ph.HE].
- [31] O. Korobkin, S. Rosswog, A. Arcones, and C. Winteler, *Mon. Not. R. Astron. Soc.* **426**, 1940 (2012).
- [32] S. Rosswog, J. Sollerman, U. Feindt, A. Goobar, O. Korobkin, C. Fremling, and M. Kasliwal, ArXiv e-prints (2017), arXiv:1710.05445 [astro-ph.HE].
- [33] S. Rosswog, U. Feindt, O. Korobkin, M. R. Wu, J. Sollerman, A. Goobar, and G. Martinez-Pinedo, *Class. Quant. Grav.* **34**, 104001 (2017).
- [34] J. J. Mendoza-Temis, M.-R. Wu, K. Langanke, G. Martínez-Pinedo, A. Bauswein, and H.-T. Janka, *Phys. Rev. C* **92**, 055805 (2015).
- [35] P. Moller, J. R. Nix, W. D. Myers, and W. J. Swiatecki, *Atom. Data Nucl. Data Tabl.* **59**, 185 (1995).
- [36] J. Duflo and A. P. Zuker, *Phys. Rev. C* **52**, R23 (1995).
- [37] S. Wanajo, Y. Sekiguchi, N. Nishimura, K. Kiuchi, K. Kyutoku, and M. Shibata, *Astrophys. J.* **789**, L39 (2014).
- [38] N. Vassh *et al.*, (2018), arXiv:1810.08133 [nucl-th].
- [39] It is interesting to note that ^{254}Cf was proposed to power the lightcurves of type Ia supernovae [47].
- [40] M. Tanaka *et al.*, *Publ. Astron. Soc. Jap.* **69**, 102 (2017).
- [41] M. Tanaka, K. Hotokezaka, K. Kyutoku, S. Wanajo, K. Kiuchi, Y. Sekiguchi, and M. Shibata, *Astrophys. J.* **780**, 31 (2014), arXiv:1310.2774 [astro-ph.HE].
- [42] C. Sneden, J. J. Cowan, and R. Gallino, *Annu. Rev. Astron. Astrophys.* **46**, 241 (2008).
- [43] S. Goriely, *Astron. and Astrophys.* **342**, 881 (1999).
- [44] J. J. Cowan, C. Sneden, T. C. Beers, J. E. Lawler, J. Simmerer, J. W. Truran, F. Primas, J. Collier, and S. Burles, *Astrophys. J.* **627**, 238 (2005), arXiv:astro-ph/0502591 [astro-ph].
- [45] W. E. Kerzendorf, C. McCully, S. Taubenberger, A. Jerkstrand, I. Seitenzahl, A. J. Ruiter, J. Spyromilio, K. S. Long, and C. Fransson, *Mon. Not. Roy. Astron. Soc.* **472**, 2534 (2017).
- [46] C. Fransson and C. Kozma, *Astrophys. J.* **408**, L25 (1993); C. Fransson and A. Jerkstrand, *Astrophys. J.* **814**, L2 (2015).
- [47] G. R. Burbidge, F. Hoyle, E. M. Burbidge, R. F. Christy, and W. A. Fowler, *Phys. Rev.* **103**, 1145 (1956).
- [48] Decay Radiation database version of 1/3/2018, https://www.nndc.bnl.gov/nudat2/indx_dec.jsp.
- [49] R. Brandt, S. G. Thompson, R. C. Gatti, and L. Phillips, *Phys. Rev.* **131**, 2617 (1963).
- [50] G. Audi, F. G. Kondev, M. Wang, W. J. Huang, and S. Naimi, *Chin. Phys.* **C41**, 030001 (2017).
- [51] JINA Reaclib, <https://jinaweb.org/reactlib/db>.
- [52] K.-W. Chan and R. E. Lingenfelter, *Astrophys. J.* **405**, 614 (1993).

Supplemental Material

Nuclei relevant for late-time kilonova lightcurves— We list in Table II all nuclei whose half-lives $t_{1/2}$ are between 10 and 100 days with atomic mass number $A > 60$. There are in total 25 isotopes and 22 decay sequences. In addition, we include ^{56}Ni , ^{66}Ni , ^{72}Zn , ^{222}Rn , and ^{224}Ra despite the fact that their $t_{1/2}$ are smaller than 10 days. This is because they can produce particular lightcurve features even at the early times, due to their relatively large energy release per decay. For example, ^{56}Ni and ^{66}Ni are the main nuclei that contribute to heating for model D at $t \lesssim 10$ days. In model C, it is instead mainly powered by the decay of ^{66}Ni and ^{72}Zn .

Among the listed nuclei, the four decay chains starting from ^{222}Rn , ^{224}Ra , ^{223}Ra and ^{225}Ra contain 3–4 α -decays and release ~ 20 –30 MeV decay energy in each. If these nuclei can be produced in an amount at the abundance level of $\sim 10^{-5}$, they can generate distinct features in the late-time lightcurve between 3 – 200 days as discussed in the paper. Moreover, the spontaneous fission of ^{254}Cf releases a even larger decay energy of ~ 185 MeV. Therefore, a late-time feature shown in the kilonova lightcurve at $t \gtrsim 50$ days can point to the production level of $\sim 10^{-6}$.

We also note here again that in the list, there are no nuclei with 10 days $< t_{1/2} < 50$ days for $A < 100$. If the merger ejecta contains mostly high Y_e material such that nuclei with this mass range are primarily produced, a dip feature in the lightcurve around 25 days is expected to be identified as discussed in the paper.

Modeling of the r -process and the radioactive decay— To model the r -process heating rate \dot{Q} in the expanding ejecta of total mass M_{ej} and average expansion velocity v_{ej} , we calculate the radioactive decay energy release rate per unit mass from a decay channel i (including β^- decay, β^+ decay/electron capture, α decay and spontaneous fission), \dot{q}_i , assuming that the material contains a Y_e distribution,

$$\dot{q}_i(t) = \int \dot{q}_i(t, Y_e) G(Y_e | Y_{e,c}, \Delta Y_e^2) dY_e, \quad (2)$$

where $G(Y_e | Y_{e,c}, \Delta Y_e^2)$ is the normalized Gaussian distribution characterized by a central value $Y_{e,c}$ and a width ΔY_e .

As the Y_e -dependent heating rate $\dot{q}_i(t, Y_e)$ at the time scale of $\sim 1 - 100$ days are completely determined by the abundance distribution of nuclei produced during the r -process nucleosynthesis, the abundances are computed by following the evolution of all nuclear species from high temperature of ~ 10 GK, when the nuclear composition is given by the nuclear statistical equilibrium, to several Gyr, using an established r -process nuclear reaction network (see e.g., Ref. [22, 34]).

The reaction network contains all relevant reactions, including charged particle reactions, neutron captures and their inverse reactions, as well as the β^- decays, α decays, β^+ decays/electron captures, and the spontaneous, β -decay induced, and neutron-capture induced fission reactions. For all the theoretical reaction rates of neutron captures and the inverse photo-dissociations, β^- decays, α decays, and fissions, we use those documented in [34]. For the experimentally-known decay rates, we adopt the most-updated ones compiled by [50]. Other reactions rates are taken from the JINA Reaclib Database of the Version v2.3 [51].

The expansion history of the ejecta used in the r -process calculation is modeled by an analytically parametrized form used in Ref. [20], characterized by the early-time expansion timescale τ_{dyn} and the entropy per nucleon s . For the results shown in the paper, we use $\tau_{\text{dyn}} = 10$ ms and $s = 10 k_B$ per nucleon, where k_B is the Boltzmann constant. The late-time shape of the heating rates does not sensitively depend on this particular choice of τ and s . For example, Fig. 5 shows the total specific rate of the radioactive energy release per unit mass $\dot{q}(t) \equiv \sum_i \dot{q}_i(t)$ for the combinations of $(s[k_B], \tau_{\text{dyn}}[\text{ms}]) = (10, 10)$, $(10, 31.62)$, $(20, 10)$, and $(20, 31.62)$ for different Y_e distributions that correspond to the models in the paper. It shows that despite the fact that the amount of late-time radioactive energy release rate scales directly with the produced amount of nuclei which can decay over that timescale, the shape remains in all cases. This further illustrates the possibility of using the late-time lightcurve shape to infer which specific nuclei are present in the ejecta, as discussed in the paper.

Modeling of the particle thermalization— The fraction of energy from decay products (photons, e^\pm , α 's and fission fragments) converted to heat (“thermalized”) in the ejecta depends on the bulk ejecta properties M_{ej} and v_{ej} , and on the type of particle emitted, the emission spectrum of each particle type, and the rate at which the radioactivity produces energy.

We model the thermalization efficiencies of β^- decay electrons and γ -rays by interpolating parametrized fits to the results of Ref. [23], which numerically calculated energy deposition assuming that the energy released by β^- decay evolved in time as a power law $\dot{q}_\beta(t) \propto t^{-1.2}$. The numerical results were found to be well described by

$$f_{e^-}(t) = \frac{\ln(1 + at^b)}{at^b}, \quad (3)$$

and

$$f_\gamma(t) = 1 - \exp \left[- \left(\frac{t_\gamma}{t} \right)^d \right], \quad (4)$$

TABLE II. The decay property of r -process nuclei with half-lives $t_{1/2} = 10 - 100$ days plus selected decays discussed in the main paper (from [48]). Nuclei that are blocked by long-lived ($t_{1/2} \gg 100$ days) preceding isotopes are excluded. Q is the total energy released per decay (chain). E_α , E_e , E_γ are the total kinetic energy per decay (chain) carried by the α , e^\pm and photons, respectively. For the spontaneous fission of ^{254}Cf , the kinetic energy E_{Kinetic} carried by the fission fragments is taken from Ref. [49]. No data is available for the neutron and photon effective energies but they are expected to be much smaller.

Isotope	Decay channel	$t_{1/2}$ (d)	Q (MeV)	E_α (MeV)	E_e (MeV)	E_γ (MeV)
^{56}Ni	EC	6.075(10)	2.133	-	-	1.721
^{56}Co	EC, β^+	77.236(26)	4.567	-	0.121	3.607
^{66}Ni	β^- to ^{66}Zn	2.2750(125)	2.893	-	1.1396	0.098
^{72}Zn	β^-	1.937(4)	0.443	-	0.080	0.152
^{72}Ga	β^-	0.587(4)	3.998	-	0.468	2.767
^{224}Ra	$\alpha\beta^-$ to ^{208}Pb	3.6319(23)	30.875	26.542	0.891	1.474
^{222}Rn	$\alpha\beta^-$ to ^{210}Pb	3.8215(2)	23.826	19.177	0.949	1.715
^{225}Ra	β^-	14.9(2)	0.356	-	0.097	0.012
^{225}Ac	$\alpha\beta^-$ to ^{209}Bi	10.0(1)	30.196	27.469	0.632	0.046
^{246}Pu	β^- to ^{246}Cm	10.84(2)	2.778	-	0.504	1.123
^{147}Nd	β^-	10.98(1)	0.895	-	0.232	0.144
^{223}Ra	$\alpha\beta^-$ to ^{207}Pb	11.43(5)	29.986	26.354	0.937	0.304
^{140}Ba	β^- to ^{140}Ce	12.7527(23)	4.807	-	0.809	2.490
^{143}Pr	β^-	13.57(2)	0.934	-	0.215	-
^{156}Eu	β^-	15.19(8)	2.452	-	0.430	1.235
^{191}Os	β^-	15.4(1)	0.314	-	0.125	0.074
^{253}Cf	β^-	17.81(8)	0.291	-	0.074	-
^{253}Es	α	20.47(3)	6.739	6.587	-	-
^{234}Th	β^- to ^{234}U	24.10(3)	2.468	-	0.860	0.016
^{233}Pa	β^-	26.975(13)	0.570	-	0.065	0.218
^{141}Ce	β^-	32.511(13)	0.583	-	0.145	0.077
^{103}Ru	β^-	39.247(3)	0.765	-	0.0638	0.497
^{255}Es	$\alpha\beta^-$ to ^{251}Cf	39.8(12)	7.529	6.968	0.175	0.021
^{181}Hf	β^-	42.39(6)	1.035	-	0.198	0.532
^{203}Hg	β^-	46.594(12)	0.492	-	0.095	0.238
^{89}Sr	β^-	50.563(25)	1.499	-	0.587	0.0
^{91}Y	β^-	58.51(6)	1.544	-	0.603	0.0
^{95}Zr	β^-	64.032(6)	1.126	-	0.117	0.733
^{95}Nb	β^-	34.991(6)	0.926	-	0.043	0.764
^{188}W	β^- to ^{188}Os	69.78(5)	2.469	-	0.878	0.061
^{185}W	β^-	75.1(3)	2.469	-	0.127	-
Isotope	Decay channel	$t_{1/2}$ (d)	Q (MeV)	E_{Kinetic} (MeV)	E_n (MeV)	E_γ (MeV)
^{254}Cf	Fission	60.5(2)	-	185(2)	-	-

where t is the post-merger time in days. The fit coefficients vary fairly smoothly with ejecta parameters, allowing them to be estimated for combinations of M_{ej} and v_{ej} not directly calculated by Ref. [23]. Table III gives a , b , t_γ , and d for each $(M_{\text{ej}}, v_{\text{ej}})$ considered in this work.

Figure 6 presents numerical results for electron and γ -ray thermalization from Ref. [23] compared to the best-fit analytic expressions calculated with Eqs. (3) and (4) for

select ejecta models similar to those studied here. Also shown are the interpolated $f_{e^-}(t)$ and $f_\gamma(t)$ for the models considered in this work. As shown in Figure 6, $f(t)$ evolves smoothly with bulk ejecta properties, enabling confident interpolation of fit coefficients between models.

The total instantaneous thermalization efficiency for β^- -decays is then

$$f_\beta(t) = 0.25f_{e^-}(t) + 0.4f_\gamma(t), \quad (5)$$

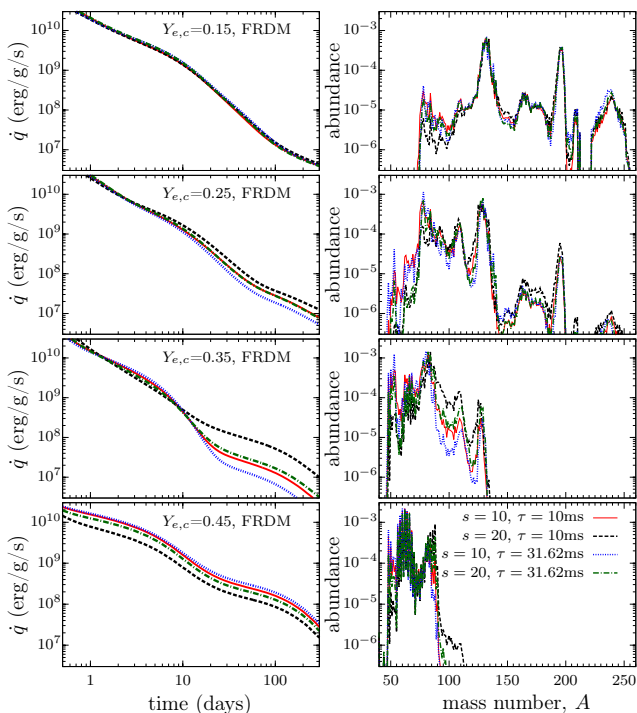


FIG. 5. The total specific rate of the radioactive energy release per unit mass $\dot{q}(t) \equiv \sum_i \dot{q}_i(t)$ (left panels) and the r -process nucleosynthesis abundances (right panels) for different Y_e distributions with various combinations of entropy s and the early-time expansion timescale τ_{dyn} .

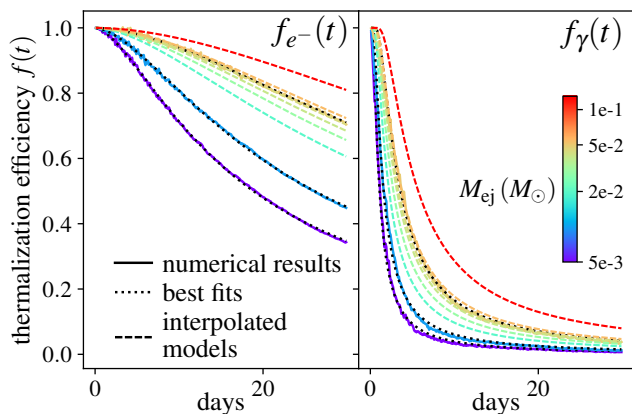


FIG. 6. Thermalization efficiencies $f(t)$ for β -decay electrons (left panel) and γ -rays (right panel). In both panels, solid, colored curves show numerical results from [23] with $v_{\text{ej}} = 0.1c$, and $M_{\text{ej}} = 0.005, 0.01, 0.05,$ and $0.1 M_{\odot}$. The best-fit analytic expressions corresponding to Eqs. (3) (left panel) and (4) (right panel) are over-plotted as dotted black lines to demonstrate the validity of the fitting function and the quality of the fit. The thermalization efficiencies for the models in this work (see Table 3) are estimated by interpolating fit coefficients as a function of ejecta parameters. The interpolated functions are plotted as dashed colored lines.

TABLE III. Coefficients for the thermalization efficiency of β -decay electrons and γ -rays

$M_{\text{ej}}(M_{\odot})$	$v_{\text{ej}}(c)$	$a(10^{-3})$	b	t_{γ} (days)	d
0.020	0.1	4.76	1.70	1.68	1.28
0.030	0.1	3.37	1.73	2.06	1.28
0.040	0.1	2.64	1.76	2.38	1.28
0.045	0.1	2.39	1.76	2.52	1.28
0.055	0.1	2.01	1.78	2.79	1.28
0.130	0.1	0.97	1.84	4.28	1.28

where the coefficients 0.25 and 0.4 approximate the partition of the decay energy into e^- and γ 's (with the remaining energy lost to neutrinos, which escape the ejecta without thermalizing). For the results presented in this paper, we do not use the detailed branching information provided in table II. However, this information will be useful for future observations.

We find that the energy produced by α -decays and fission is dominated by a handful of decay chains, and therefore does not follow a power-law. Thermalization is sensitive to the form of $\dot{q}(t)$ [24], particularly at the late times we are probing in this paper. Therefore, instead of adopting the results of [23], we have directly calculated $f_{\alpha}(t)$ and $f_{\text{fiss}}(t)$ for the *individual* nuclei most important for heating by these channels.

The procedure for these calculations is similar to that presented in Ref. [24]. The energy-loss rates for α particles and fission were modeled as power laws ($\dot{E}_{\alpha, \text{fiss}} \propto E^{\zeta}$), where the power-law index ζ and the coefficient of proportionality were chosen based on the detailed energy-loss rates compiled by Ref. [23]. For α -particles, we estimate $\dot{E}_{\alpha} = 5 \times 10^{11} \rho(t) \text{ MeV s}^{-1}$ ($\zeta = 0$), while for fission fragments we find $\dot{E}_{\text{fiss}} = 4.5 \times 10^{13} (E_{\text{fiss}}/A) \times \rho(t) \text{ MeV s}^{-1}$, where A is the fragment's mass number and ρ is in units of g cm^{-3} . In both cases, we adopt a uniform density: $\rho = 3M_{\text{ej}}/4\pi v_{\text{ej}}^3 t^3$.

These simplifications allow the analytic expression of a particle's energy evolution with time, given its initial energy E_0 , its birth time t_1 , and the current time t . The instantaneous deposition of energy associated with any particular decay in a decay chain can be solved numerically by calculating

$$\dot{q}_{\text{dep}}(t) = \int_{t_1}^t \dot{n}(t'_1) \dot{E}(E(t, t'_1)) dt'_1, \quad (6)$$

with the associated thermalization efficiency given by

$$f(t) = \frac{\dot{q}_{\text{dep}}(t)}{\dot{q}_{\text{rad}}(t)} = \frac{\int_{t_1}^t \dot{n}(t'_1) \dot{E}(E(t, t'_1)) dt'_1}{E_0 \dot{n}(t)}. \quad (7)$$

In Eqs. (6) and (7), the lower limit t_1 is the birth time of the oldest particle not completely thermalized at time t , and $\dot{n}(t)$ is the rate of particle emission.

In the case of ^{254}Cf , $\dot{n}(t)$ is an exponential. Because fission fragment thermalization is sensitive to the fragment's mass and energy, we adopt a simplified model of the ^{254}Cf fission fragment distribution, in which every fission event produces a heavy and a light fragment whose properties are the most probable values measured by Ref. [49]. The light (heavy) fragment has atomic number, mass number, and kinetic energy 42, 109, and 102 MeV (56, 145, and 80 MeV), respectively. The total $f(t)$ for ^{254}Cf is an initial energy-weighted sum of $f(t)$ for each fragment.

For α -decays, which generally occur as links in a longer decay-chain and which do not exhibit exponential decay at all times, we calculate number $N_i(t)$ of each nucleus in the chain, allowing the determination of $\dot{n}_i(t) = -N_i(t)/\tau_i$, where nucleus i has a lifetime τ_i . The thermalization efficiency for the entire chain is simply a sum over its constituent α -decays,

$$f_{\text{tot},\alpha}(t) = \frac{\sum_i f_i(t) E_{0,i} \dot{n}_i(t)}{\sum_i E_{0,i} \dot{n}_i(t)}. \quad (8)$$

Many of the decay chains that produce α -particles also contain nuclei that undergo β^- -decay. Because the electrons emitted in these decays have energies that are comparable to those of β -decay electrons from other r -process nuclei emitted at similar times, we consider these electrons as forming part of the β -decay background, and absorb them into the general calculation of β -decay thermalization (Eq. (5)).

Figure 7 illustrates the impact of the heating rate \dot{q}_{rad} on the form of $f(t)$. We show, for an ejecta model with $(M_{\text{ej}}, v_{\text{ej}}) = (0.01 M_{\odot}, 0.1 c)$, numerical results for α particles computed assuming a power-law heating rate, compared to the semi-analytic $f(t)$ for a representative α -decay chain, ^{223}Ra , calculated as described above.

In general, the contribution of partially-thermalized particles emitted at earlier epochs causes $f(t)$ to decrease more slowly than $\dot{q}_{\text{rad}}(t)$. However, this effect is particularly strong for exponential decays, where the instantaneous energy deposition can actually exceed the instantaneous energy production, leading to $f(t) > 1$, as shown in Figure 7. The exponential (or quasi-exponential) decay rates in the case of ^{223}Ra result in a less steep decline at intermediate times, and cause $f(t) \rightarrow \infty$ as $t \rightarrow \infty$. While the position and depth of the local minimum depend on ejecta parameters and the Q -values and timescales of the decays in question, the asymptotic behavior is a robust feature of single-isotope/single-decay chain heating. Despite the asymptotic behavior of $f(t)$ in this regime, $\dot{q}_{\text{rad}}(t) \times f(t)$ remains finite at all times and asymptotes to a power-law as $t \rightarrow \infty$ [24], and the time-integrated deposited energy is less than the total radiated energy.

In compositions neutron-poor enough to synthesize ^{56}Ni , the decay of the ^{56}Ni daughter ^{56}Co proceeds via

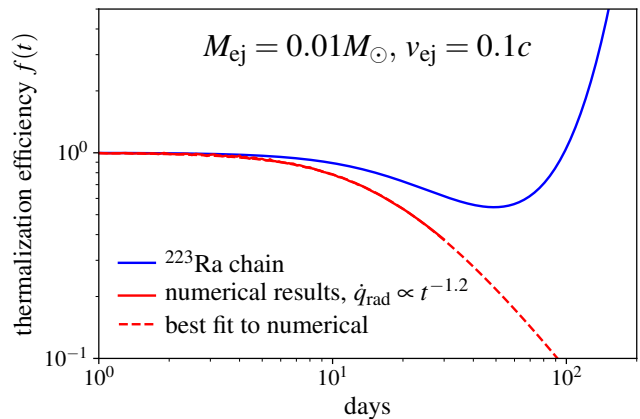


FIG. 7. The effect of \dot{q}_{rad} on $f(t)$. The red curve shows the numerical results of [23] for α -particle thermalization assuming power-law heating, $\dot{q}_{\text{rad}} \propto t^{-1.2}$. An analytic fit to the numerical results, calculated using Eq. 3 (dashed red line), has been used to extend the curve past $t = 30$ days. (The continual decrease of $f(t)$ for power-law heating is expected analytically, and is not imposed by our choice of fitting function.) For comparison, we plot in blue the thermalization efficiency calculated using Eq. 7 for the α -particles produced by the decay chain originating with ^{223}Ra , which shows qualitatively different behavior. The two curves begin to diverge around $t = 5$ days, and the discrepancy increases with time.

β^+ decay with a branching ratio of 19%, creating a population of high-energy positrons that carry $\sim 3\%$ of the total decay energy. Most of the energy (79%) is carried by γ -rays, with neutrinos accounting for the remainder. As with electrons, the primary channel for positron energy loss is Bethe-Bloch interactions [52]; however, as a result of different relativistic corrections to the Bethe-Bloch formula for electrons and positrons, the energy-loss rates for positrons with energies near 1 MeV are slightly higher than those for electrons.

We find that the energy-loss rate for positrons varies roughly as $E^{-1/4}$ in the energy range of interest. We then calculate the thermalization efficiency of positron energy, $f_{e^+}(t)$, as described above for α -particles and fission fragments. The total thermalization efficiency of the $^{56}\text{Ni} \rightarrow ^{56}\text{Co} \rightarrow ^{56}\text{Fe}$ chain is approximately

$$f_{\beta^+/\text{EC}}(t) = 0.03f_{e^+}(t) + 0.79f_{\gamma}(t). \quad (9)$$

Inferring U and Th abundances— We discuss in this section the possibility of inferring the U and Th abundances utilizing the (non-)detection of the lightcurve signature of translead nuclei. Taking GW170817 as an example, the produced abundance of $A = 222$ – 225 nuclei can be estimated to be smaller than $\sim 10^{-5}$. One can then take a model among those with varying composition and nuclear input, which predicts the largest ratio of nuclei that eventually decay to the U/Th abundances relative to the $A = 222$ – 225 nuclei, to infer a “model-dependent” upper limit for the amount of U and Th pro-

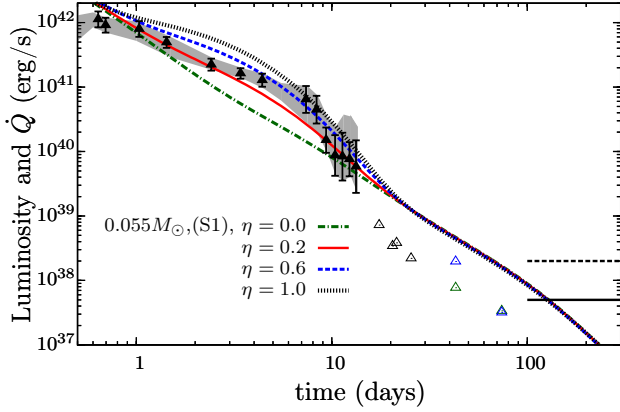


FIG. 8. Heating rate powered by the Solar- r abundances distribution for nuclei between $69 \leq A \leq 205$ from the abundance set S1 [42]. Due to the large uncertainty of ^{72}Ge abundance in different abundance sets (see paper) and its dominating role in heating, the amount of $A = 72$ nuclei has been adjusted by $Y(A = 72) = \eta \times Y(A = 72)|_{S1}$.

duced. Within the scenarios examined here, model A,

based on the FRDM nuclear masses, gives such a largest ratio with an total abundance of $\sim 10^{-5}$ (mass fraction $\sim 2.2 \times 10^{-3}$) for $A = 222\text{--}225$ nuclei, and the U/Th abundances (after decay) of $\sim 1.5 \times 10^{-4}$ (mass fraction $\sim 3.5 \times 10^{-2}$). Therefore, the upper limit on the U/Th abundances can be set to be $\sim 3.5 \times 10^{-2}$, which translates to a total amount of $\sim 1.75 \times 10^{-3} M_{\odot}$ when taking $M_{\text{ej}} \sim 0.05 M_{\odot}$.

Similarly, a future (non-)observation of the feature of ^{254}Cf may likewise be used to determine the U/Th yield.

Solar r -abundances of ^{72}Ge and GW170817— As discussed in the paper, the amount of ^{72}Ge in the Solar r -process abundances, which is uncertain, plays a key role in connecting the Solar r -process abundances with the GW170817 kilonova lightcurve. Fig. 8 further shows the comparison of the L_{bol} of AT 2017gfo with \dot{Q} powered by the β -decay of nuclei that follow the Solar r -process distribution for $69 \leq A \leq 205$, with the amount of $Y(A = 72) = \eta \times Y(A = 72)|_{S1}$, for a fixed ejecta mass $M_{\text{ej}} = 0.55 M_{\odot}$. It shows that even with such large M_{ej} , it requires $\eta \gtrsim 0.2$ to power the observed lightcurve, if we demand that GW170817 produces the entire range of the r -process nuclei.